Journal of Computational and Applied Mathematics 230 (2009) 656–673

Contents lists available at ScienceDirect

Journal of Computational and Applied Mathematics

journal homepage: www.elsevier.com/locate/cam

Numeric treatment of contact discontinuity with multi-gases

Tzong-Hann Shieh [a,*], Meng-Rong Li [b]

[a] Department of Aerospace and Systems Engineering, Feng Chia University, No. 100, Wenhwa Road, Seatwen, Taichung 40724, Taiwan, ROC

[b] Department of Mathematical Sciences, National Chengchi University, No. 64, Sec. 2, ZhipNan Road, Wenshan District, Taipei 11605, Taiwan, ROC

ARTICLE INFO

Article history:
Received 11 June 2007
Received in revised form 12 August 2008

MSC:
76N15
35L65
35L67

Keywords:
FVM
Euler equations
Contact discontinuity
Multi-gases

ABSTRACT

In this paper we work with a finite-volume-procedure for the computation of the one-dimensional Euler equations for the treatment of multi-gases and the problem of the correct treatment of the discontinuity was more nearly investigated. A suggested equation was embedded in the finite volumes context and implemented in our code accordingly and regarded as validated.

1. Introduction

In the experimental investigation of high enthalpy flows, as they arise from the reentry of space missiles, to stand exclusion from the impulse plants, since in continuous operation, the high temperatures would bring each plant to melt; the High Enthalpy Tunnel Göttingen (HEG) of the German Aerospace Center (DLR) - Institute for Fluidmechanics is such a plant; it is a flight-piston-driven shock tunnel, the helium being compressed as a driver gas with pressures of 50–100 MPa, before it comes into contact with the test gas air. The resulting unsteady flow field – particularly the movement of the contact surface between the gases – is very important for the operation of the plant.

During the numerical simulation of contact surfaces between different gases with the usual procedures, some non-physical disturbances in direct proximity of the contact discontinuity and shocks arise. The deviations lie in the percent range of the states before and behind the contact discontinuity.

The further cause of this problem produces another computation structure of the usual procedures. In each time step, the flux-balances are accomplished with the cell borders and are used for the determination of a cell average value in the next time step. Such a cell average value can represent a state, if a discontinuity runs through the cell, it will have nothing to do with the flow field here.

To study the above problem, some authors [1–6] have pointed out some different directions and in some solution spaces, in particular, the analysis used in [5] is needed in this study. Ton attributes the non-physical disturbances to an inconsistency of the mixture formula for the relationship of specific heat, arising in different temperatures by the gases involved. He suggests a more general mixture formula, which reduces to the usual formula, if all the gases have the same temperature. In order to solve this general mixture formula, the partial pressures P_i are needed, which Ton obtained from additional energy equations of the species.

* Corresponding author. Tel.: +886 4 24517250x3960; fax: +886 4 24510862.
E-mail addresses: thshieh@fcu.edu.tw (T.-H. Shieh), liwei@math.nccu.edu.tw (M.-R. Li).

0377-0427/$ – see front matter © 2009 Elsevier B.V. All rights reserved.
doi:10.1016/j.cam.2009.01.014

Our primary goal is to continue developing a code regarding the problems described above based on the examples of the moving contact discontinuities and a shock tube. In addition, the relevant gas dynamics magnitudes of the one-dimensional, frictionless, compressible and unsteady flow of a gas mixture are treated with the help of a finite volume procedure.

This second order Upwind procedure for the solution of the one-dimensional Euler equations for an ideal gas has an explicit two-stage Runge Kutta procedure for the time discretization, a MUSCL reconstruction with TVD Limiter for the spatial discretization and a AUSMDV Riemann solvers. This procedure is to be extended to the treatment on the multi-gases and to investigate the problems described above.

2. Physical modeling

The numerical simulation of flows is based on the physical (and chemical) models. The mathematical models are formulated by some partial differential equations, in terms of spatial and temporal changes of the flow parameters. The frictionless gas dynamics plays a special role by the physical conservation equations with a hyperbolic character. On the one hand, the equations describe the substantial phenomenon of wave propagation and on the other hand the non-linearity arises from the time-dependent and the compressible flow; they include also discontinuity, i.e. shocks and contact discontinuity; such flow-mechanical principal equations have already been described in the literature by [7–12].

The basis of this work is the acceptance of a mixture of ideal gases in a frictionless, unsteady one-dimensional flow. The Euler equations are thus applied here neglecting excitation- and ionization-processes, outside forces (i.e. volume forces such as gravitation, electromagnetic fields etc.), as well as chemical reactions.

2.1. The Euler equations

The conservation equations can be deduced in principle from the integrals expressions, under the condition that the temporal derivatives are exchangeable with the spatial integrations, i.e. the integrands are continuous differentiable in t, which can be written as follows:

$$\frac{\partial \rho}{\partial t} + \frac{\partial}{\partial x}(\rho u) = 0, \tag{1}$$

$$\frac{\partial \rho_i}{\partial t} + \frac{\partial}{\partial x}(\rho_i u) = 0, \tag{2}$$

$$\frac{\partial (\rho u)}{\partial t} + \frac{\partial}{\partial x}(\rho u u) + \frac{\partial}{\partial x} P = 0, \tag{3}$$

$$\frac{\partial (\rho E)}{\partial t} + \frac{\partial}{\partial x}[(\rho E + P)u] = 0. \tag{4}$$

To derive an additional energy equation for a species i in the next section we will use the Euler equations.

2.2. Energy equation of a species

In this paper, we use the models extended in [5,13] and the additional energy equation of a species i is derived in the following way in one-dimensional case:

The total energy ρE consists of the internal energy and the kinetic energy

$$\rho E = \rho e + \frac{1}{2}\rho u^2, \tag{5}$$

where E is the total energy per mass unit, e the internal energy per mass unit and u the velocity. We apply the above equation to the energy conservation (4), afterwards we can derive the derivatives $\frac{\partial(\rho u)}{\partial t}$, $\frac{\partial u}{\partial t}$ and further conservation equations on the mass and momentum.

Thus, the following equation results by the specific internal energy. By (4) and (5) we have

$$e\frac{\partial \rho}{\partial t} + \rho\frac{\partial e}{\partial t} + \frac{1}{2}u^2\frac{\partial \rho}{\partial t} + \rho u\frac{\partial u}{\partial t} + u\frac{\partial}{\partial x}\left(\rho e + \frac{1}{2}\rho u^2 + P\right) + \left(\rho e + \frac{1}{2}\rho u^2 + P\right)\frac{\partial}{\partial x}u = 0,$$

$$\rho\frac{\partial e}{\partial t} + \left(e + \frac{1}{2}u^2\right)\frac{\partial \rho}{\partial t} + u\left[\frac{\partial(\rho u)}{\partial t} - u\frac{\partial \rho}{\partial t}\right] + u\frac{\partial}{\partial x}\left(\rho e + \frac{1}{2}\rho u^2 + P\right) + \left(\rho e + \frac{1}{2}\rho u^2 + P\right)\frac{\partial}{\partial x}u = 0.$$

According to (1) and (3), the above equation can be rewritten in the following form:

$$\rho\frac{\partial e}{\partial t} + \left(e - \frac{1}{2}u^2\right)\left[-\frac{\partial}{\partial t}(\rho u)\right] + u\left[-\frac{\partial}{\partial t}(\rho u^2) - \frac{\partial}{\partial t}P\right] + u\frac{\partial}{\partial x}\left(\rho e + \frac{1}{2}\rho u^2 + P\right) + \left(\rho e + \frac{1}{2}\rho u^2 + P\right)\frac{\partial}{\partial x}u = 0,$$

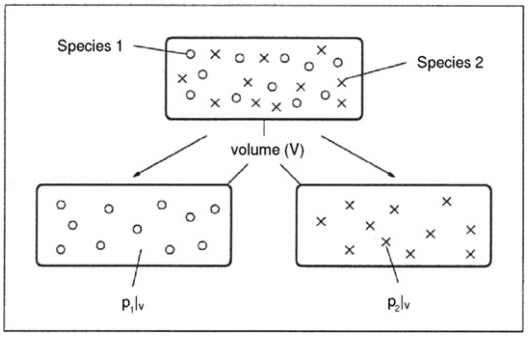

Fig. 1. Definition of the partial pressure P_i.

$$\rho\frac{\partial e}{\partial t}+\left(\frac{1}{2}u^2-e\right)\left[\frac{\partial}{\partial t}(\rho u)\right]-\frac{1}{2}u\frac{\partial}{\partial x}(\rho u^2)+u\frac{\partial}{\partial x}(\rho e)+\left(\rho e+\frac{1}{2}\rho u^2+P\right)\frac{\partial}{\partial x}u=0,$$
$$\rho\frac{\partial e}{\partial t}-e\left[\frac{\partial}{\partial x}(\rho u)\right]+u\frac{\partial}{\partial x}(\rho e)+\rho e\frac{\partial}{\partial x}u+P\frac{\partial}{\partial x}u=0,$$
$$\rho\frac{\partial e}{\partial t}-eu\frac{\partial}{\partial x}\rho-e\rho\frac{\partial}{\partial x}u+u\rho\frac{\partial}{\partial x}e+ue\frac{\partial}{\partial x}\rho+\rho e\frac{\partial}{\partial x}u+P\frac{\partial}{\partial x}u=0,$$
$$\frac{\partial e}{\partial t}+u\frac{\partial}{\partial x}e+\frac{P}{\rho}\frac{\partial}{\partial x}u=0.$$

Denoted by

$$\frac{\mathrm{D}}{\mathrm{D}t}:=\frac{\partial}{\partial t}+u\frac{\partial}{\partial x},$$

with the help of Eq. (1), we obtain further

$$\begin{aligned}0&=\frac{\partial e}{\partial t}+u\frac{\partial e}{\partial x}+\frac{P}{\rho}\left[-\frac{1}{\rho}\left(\frac{\partial\rho}{\partial t}+u\frac{\partial\rho}{\partial x}\right)\right]\\&=\left(\frac{\partial e}{\partial t}+u\frac{\partial e}{\partial x}\right)-\frac{P}{\rho^2}\left(\frac{\partial\rho}{\partial t}+u\frac{\partial\rho}{\partial x}\right)\\&=\frac{\mathrm{D}e}{\mathrm{D}t}-\frac{P}{\rho^2}\frac{\mathrm{D}\rho}{\mathrm{D}t}.\end{aligned}\tag{6}$$

In order to transform this equation into an equation for the internal energy of a species, we need the partial pressure P_i and the partial density ρ_i of the species i and the volume fraction f_i. These notions can be illustrated as follows: From a gas mixture in a volume V will leave only one species at the same temperature in the system, which is shown in the Fig. 1 [13].

The pressure adjusts itself and we will denote P_i as the partial pressure. For an ideal gas, the thermal equation can be applied to the partial pressure

$$P_i|_V=\rho_i|_V R_i T_i,$$

where R_i denotes the specific gas constants and T_i the temperatures of the species. The partial density $\rho_i|_V$ is defined by the mass of the species per volume M_i/V. These definitions are accordingly made out to each species. If the volume is divided by a separation of the species with constant pressure in partial volume V_i represented in the Fig. 2 [13], then it can be applied to ideal gases

$$P|_V:=P_i|_{V_i}=\frac{M_i}{V_i}R_iT_i\quad\text{and}\quad\rho|_V:=\rho_i|_{V_i}=\frac{M_i}{V_i}.$$

This results in the volume fraction f_i of a species i with $P|_V:=P|_{V_i}$ and $\rho|_V:=\rho|_{V_i}$ (see the Fig. 2)

$$f_i=\frac{V_i}{V}=\frac{M_iR_iT_i}{P|_V}\frac{P_i|_V}{M_iR_iT_i}=\left.\frac{P_i}{P}\right|_V\quad\text{and}\quad f_i=\frac{V_i}{V}=\frac{M_i}{\rho|_V}\frac{\rho_i|_V}{M_i}=\left.\frac{\rho_i}{\rho}\right|_V.$$

In the volume V_i there exists only one species, whose internal energy is therefore valid accordingly the Eq. (6)

$$\frac{\mathrm{D}e|_{V_i}}{\mathrm{D}t}-\frac{P|_{V_i}}{\rho^2|_{V_i}}\frac{\mathrm{D}\rho|_{V_i}}{\mathrm{D}t}=0.$$

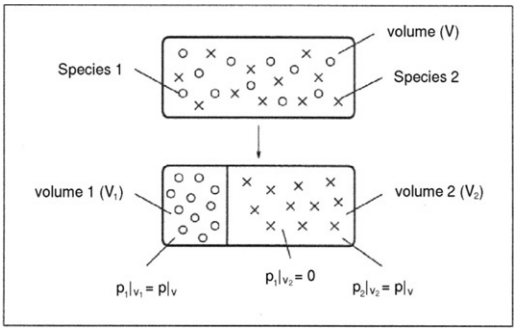

Fig. 2. Partial volume V_i of the different species.

With reference to the entire volume V, this means

$$\begin{aligned} 0 &= \frac{\mathrm{D}e_i}{\mathrm{D}t} - P_i \frac{P}{P_i}\frac{\rho_i^2}{\rho^2}\frac{1}{\rho_i^2}\frac{\mathrm{D}}{\mathrm{D}t}\left(\rho_i \frac{\rho}{\rho_i}\right) \\ &= \frac{\mathrm{D}e_i}{\mathrm{D}t} - P_i \frac{1}{f_i} f_i^2 \frac{1}{\rho_i^2}\frac{\mathrm{D}}{\mathrm{D}t}\left(\rho_i \frac{1}{f_i}\right) \\ &= \frac{\mathrm{D}e_i}{\mathrm{D}t} - \frac{P_i f_i}{\rho_i^2}\frac{\mathrm{D}}{\mathrm{D}t}\left(\frac{\rho_i}{f_i}\right). \end{aligned} \tag{7}$$

From this equation Ton had derived a additional energy equation of a species i in [5,13], which can be reformulated by our case in one-dimensional case to the additional energy equation of the species i

$$\frac{\partial(\rho_i E_i)}{\partial t} + \frac{\partial}{\partial x}(\rho_i E_i u) + Y_i u \frac{\partial}{\partial x} P + \frac{P_i P}{\gamma_i \sum_{j=1}^{ns} \frac{P_j}{\gamma_j}} \frac{\partial}{\partial x} u = 0. \tag{8}$$

This additional energy equation of the species, is independent on f_i. For gas flows of a species, this equation is identical to the conservative equation (4). To avoid the non-physical disturbances in several species of the mixed gas flows, one must discretize the Eq. (8).

2.3. Thermodynamics of the mixture of ideal gases

In this work, the contact discontinuities are considered between gases with different thermodynamic characteristics. Therefore we use two models suggested in [5,13] of the mixture formulas for γ.

The usual numerical representation is a perfect mixture with the same temperature. The usual model of the mixture shows that its equation of state is not consistent with the thermodynamics. The intention of the new numerical model is that one can interpret the mixture as a collection of species with different temperatures.

In such a model we will consider a control volume and it will be divided into sub-regions with different species; each species can have its own temperature. The equation for specific heat in the mixture can be derived with the total energy of the species i per volume, the specific enthalpy of the species i at the temperature T_i and the ideal gas law for each species is as follows

$$\gamma = 1 + \frac{P}{\sum_{i=1}^{ns} \frac{P_i}{\hat{\gamma}_i - 1}}, \tag{9}$$

where $P = \sum_{i=1}^{ns} P_i$. In the Eq. (9) we apply $\hat{c}_{p,i} = c_{p,i}$ and $\hat{\gamma}_i = \gamma_i$. This general form permits different temperatures in a cell. The equation shows that the γ-variable of the mixture is dependent on the partial pressure P_i. In order to compute the relation of specific heat γ with (9), it is necessary to know the partial pressure P_i for each species. With the acceptance of an ideal gas, the partial pressure P_i can be determined from the additional energy equation

$$P_i = (\gamma_i - 1)\left(\rho_i E_i - \frac{1}{2}\rho_i u^2\right). \tag{10}$$

In the following special case of the Eq. (9), we suppose that all species in a cell should have the same temperature. After some derivations and reformulations, we get the following model for the relationship of specific heat in the mixture

$$\gamma = 1 + \frac{\sum_{i=1}^{ns} \frac{Y_i}{W_i}}{\sum_{i=1}^{ns} \frac{Y_i}{W_i(\gamma_i - 1)}}. \tag{11}$$

This equation can also be written as follows

$$\gamma = 1 + \frac{\sum_{i=1}^{ns} \frac{\rho_i}{W_i}}{\sum_{i=1}^{ns} \frac{\rho_i}{W_i(\gamma_i - 1)}}, \tag{12}$$

which we denote the usual mixture formula as γ. We apply (11) and (12) only to a control volume, for which it can be surely accepted that all gas components have the same temperature. And then, at a contact surface between separate species develops a different temperature, this simplifying model breaks down.

2.4. Computation of the model equations

With the Eqs. (1)–(4), the discontinuity in the solution domain e.g. shocks and contact discontinuity cannot be described. Therefore the so-called weak solution of the equation-systems is considered, which also permits such discontinuity. That is, in order to treat such problems correctly, the integrals equations described before are to be used in the following investigations.

The one-dimensional Euler equations for ideal gases mixtures can be arranged in the following form:

$$\frac{\partial}{\partial t} \int_V U \mathrm{d}x + \int_{\partial V} F \mathrm{d}A = \int_V Q \mathrm{d}x, \tag{13}$$

where V represents the volume, ∂V the surface of the volume V, U the vector of the conservative variables, F the frictionless flux vector, Q the vector of the source terms and

$$U = \begin{bmatrix} \rho_i \\ \rho u \\ \rho_i E_i \\ \rho E \end{bmatrix}, \qquad F = \begin{bmatrix} \rho_i u \\ \rho u^2 \\ \rho_i E_i u \\ \rho E u \end{bmatrix} + \begin{bmatrix} 0 \\ P \\ 0 \\ Pu \end{bmatrix},$$

$$Q = \begin{bmatrix} 0 \\ 0 \\ -\left(Y_i u \frac{\partial}{\partial x} P + \frac{P_i P}{\gamma_i \sum_{j=1}^{ns} \frac{p_j}{\gamma_j}} \frac{\partial}{\partial x} u \right) \\ 0 \end{bmatrix}.$$

Here the first vector stands representatively for all species of the mixture, there the balance equations of the individual partial densities derivatives between itself only in the index. According to the third vector stands representatively for all species, for which an additional equation for the partial energy is to be solved. That is, in this study the partial densities of two species are ρ_1 and ρ_2 in the balance equations, but only arises an additional, partial energy of the species $\rho_1 E_1$, since the energy of the other species is obtained from the total energy.

The thermodynamic magnitudes of the partial pressure P_i, the total pressure P and the relationship of the specific thermal capacities γ are computed by the additional equations from Section 2.3.

3. Numeric method

In this work, the nonlinear hyperbolic equations are to be considered for spatially one-dimensional problems. The physical process in the shock tube is a typical model problem for the numerical solution. To discretize such equations we use many well-known different methods. In this work a finite volume method is used. The numerical schema ranks among the class of the *shock capturing methods*. Such methods dissolve shocks within fewer grid points.

3.1. Finite volume procedure

The finite volume procedure can be deduced from the integrals considerations. By the Eq. (13) we obtain a conservative discretization for the flow-mechanical equations [14]. The discretization schema for nonlinear differential equation systems (13) differ substantially from the methods for linear systems. Possibly the arising discontinuities also may not hurt the

principle of the conservation laws numerically. The temporal and spatial discretization effected independently, and can be described in the following way:

With this method, the entire computation field is divided into individual control volumes K (*computing cells*). The delimitations of the individual control volumes can be derived for example from the lines of the computing grid. To hold it remains that by the fixing of the discretization of the computation field, the not-overlapping control volumes are produced. The transfer of the differential equations into algebraic equations happens with this method, in which the differential equations are integrated over the individual control volumes. A precise description takes place by means of the integral form of the conservation laws, which must be applied to each closed volume Δt and Δx. From the integrals form of the conservation equations, (13) should be indicated here again

$$\frac{\partial}{\partial t}\int_K U(x,t)\mathrm{d}x + \oint_{\partial K} F(x,t)\mathrm{d}A = \int_K Q(x,t)\mathrm{d}x.$$

We can reformulate this conservation equation by a variable ϕ_K in the following way

$$\frac{\partial}{\partial t}\int_K U(x,t)\mathrm{d}x = \phi_K(t). \tag{14}$$

The term $\phi_K(t)$ is defined by

$$\phi_K(t) := \int_K Q(x,t)\mathrm{d}x - \oint_{\partial K} F(x,t)\mathrm{d}A. \tag{15}$$

For the necessary flux computation by the approximate Riemann slovers AUSMDV and the discretization of the source term $Q(x,t)$ will be treated later. The right hand side of the Eq. (14) depends on t and $\partial/\partial t$. With the definition of the cell average value of U for each control volume K given by

$$\bar{U}_K(t) := \frac{1}{|K|}\int_K U(x,t)\mathrm{d}x, \tag{16}$$

the Eq. (14) can be reformulated

$$|K|\frac{\mathrm{d}}{\mathrm{d}t}\bar{U}_K(t) = \phi_K(t).$$

In the one-dimensional case we apply here the control volume $|K| = |\Delta x| = |x_2 - x_1|$. Integrating the above equation over the time, then

$$\Delta x\int_{t_1}^{t_2}\frac{\mathrm{d}}{\mathrm{d}t}\bar{U}_K(t)\mathrm{d}t = \int_{t_1}^{t_2}\phi_K(t)\mathrm{d}t,$$

which means that

$$\Delta x\Delta\bar{U}_K = \phi_K(t_1)\Delta t,$$

where $\phi_K(t_1)\Delta t$ is an approximation of first order for the integral at the right hand side.

By

$$\Delta\bar{U}_K = \bar{U}_K(t_2) - \bar{U}_K(t_1)$$

we get a time step procedure of first order for the outgoing equation

$$\bar{U}_K(t_2) = \bar{U}_K(t_1) + \frac{\Delta t}{\Delta x}\phi_K(t_1). \tag{17}$$

The accuracy of the time discretization is increased by the fact that the values are considered between the times.

After discretization, one receives the coupled ordinary differential equations in the time for the discrete variables of state in each volume cell, which are solved with a time integration procedure, for which we use the two steps Runge Kutta method [15,16]. The Runge Kutta procedure of second order is given in the following way

$$\bar{U}_K(t_2) = \bar{U}_K(t_1) + \frac{1}{2}\frac{\Delta t}{\Delta x}\phi\left(\bar{U}_K(t_1)\right) + \frac{1}{2}\frac{\Delta t}{\Delta x}\phi\left[\bar{U}_K(t_1) + \frac{\Delta t}{\Delta x}\phi\left(\bar{U}_K(t_1)\right)\right]. \tag{18}$$

3.2. Time step procedure

Between an explicit and an implicit procedure, the temporal expenditure for an individual computation step approximately there is an order of magnitude. Therefore an explicit procedure is favorable opposite an implicit, if the time increments of both procedures are in the same order of magnitude [15]. For the running of fast unsteady processes in frictionless flow in this investigation, an explicit procedure is therefore suitable.

For an explicit procedure, the following stability condition [17] must be kept:

The Delimitation of the time step Δt in such a manner that the propagation process lies completely in the numerical dependence range. This is thus specified in first order by the neighboring grid points, thus by Δx, and by the propagation speed v. The time step delimitation is expressed in the so-called CFL-number (*Courant Friedrichs Lewy*) C_{CFL}. That is, the numerical dependence domain must contain the physical dependence domain completely [16].

The discretization of the time increment is coupled then directly to the stability condition (*CFL-condition*), at each grid point and for each time steps the explicit time intended those as follows

$$\Delta t = \frac{\Delta x}{\upsilon_{\max}} C_{CFL}. \tag{19}$$

Here Δx denotes the linear dimension of the control volume and $\upsilon_{\max}$ the maximum propagation velocity for information within the control volume, is given by $|\underline{u}| + c$. In addition, the explicit procedure remains stable for CFL-numbers between $0 \leq C_{CFL} \leq 1$. Generally, a value of the CFL-number is aimed at nearby 1. The smallest locally computed time step $\Delta t_{\min}$ for all control volumes in an time accurate is used as explicit procedure [15].

3.3. Reconstruction

The MUSCL reconstruction method (*Monotone upstream-centered Schemes for Conservation Laws*) was developed from V. Leer as an extension of the method derived by Godunov for second order. The basic idea of this method has to replace the piecewise constant distribution of the variables of state in the cells by a piecewise linear distribution. The interactions between two neighboring cells become thereby more varied and can be the only numerically determined approach.

Numerical methods of first order are always monotonous receiving, i.e., their solutions are free in the environment of discontinuity from unwanted oscillations. An extension procedure of second order in the spatial discretization can lead to difficulties, since that by each procedure of second order the instability of the solution in its environment causes the non-physical oscillations. In order to avoid these phenomena, we use a nonlinear limitation, those the procedure at extrema reduced a method of first order [15].

3.3.1. Gradients and Limiter

The simple difference for the gradient computation leads to a procedure of second order. The gradient of U reads then

$$\left(\frac{\partial U}{\partial x}\right)\bigg|_{x_i} = \frac{\Delta U_i}{\Delta x_i}, \tag{20}$$

where $\Delta U_i = U(x_{i-1}) - U(x_i)$ and $\Delta x_i = x_{i-1} - x_i$.

However such a method affects the instability, i.e., it produces unwanted non-physical oscillations nearby the shock front and the contact discontinuity. In order to avoid these phenomena, a controlled influence on the reconstruction must be taken. Essentially, the method of the so-called TVD condition (*Total Variation Diminishing*) should be sufficient. A function given on a grid $U(x, t)$, is defined as the total variation of the function [16]

$$TV\,[U(,t)] = \sup_{(\text{over all grid points } x_i)} \sum_{i=-\infty}^{\infty} |U(x_{i+1}, t) - U(x_i, t)|, \tag{21}$$

where t is the time step. If the numerical treatment is TVD, then applies

$$TV\,[U(,t_{i+1})] \leq TV\,[U(,t_i)]\,. \tag{22}$$

The above condition means that the total variation (TV) of a solution with increasing time step does not increase. In the environment of a discontinuity leads to the oscillation-free solutions. The associated numerical schemes are called TVD schemes.

A transmission to one-dimensional systems is possible in principle by means of the Riemann variables. The limiter-functions compute a factor Ψ on the basis of one-sided gradients in the neighboring cells, the gradient must be multiplied in the reconstruction step, this means that

$$U(x) = \bar{U} + \Psi \left(\frac{\partial U}{\partial x}\right)(x - \bar{x}).$$

Here the *minmod*-function is defined by

$$\Psi_K(a, b) = \operatorname{minmod}(a, b) = \begin{cases} a : ab > 0 \quad \text{and} \quad |a| \leq |b|, \\ b : ab > 0 \quad \text{and} \quad |a| > |b|, \\ 0 : ab \leq 0. \end{cases} \tag{23}$$

Here denoted by a and b the one-sided gradients of the variable, which (20) are also computed as $\left(\frac{\partial U}{\partial x}\right)|_{x_i}$ and $\left(\frac{\partial U}{\partial x}\right)|_{x_{i+1}}$.

The interpolations are not carried out with the state vector of the conservative variable $(\rho_1, \rho_2, \rho u, \rho E_1, \rho E)$ directly, but rather the conservative magnitudes converted first into primitive variables in all involved grid points, their vectors are given by $(\rho_1, \rho_2, u, p_1, p_2)$. All operations are then carried out with such vector.

3.4. Numeric flux function: Approximate Riemann Solver-AUSMDV

In order to solve this problem accurately, it must however be determined iteratively. Such an accurate solution needs some complex iterative computations, and still some problems remain. After the integration over the control volumes, it remains a large part of the information of the accurate solution of the individual Riemann-problems that are unused; for this reason a large number of different approximate Riemann solvers in the literature were developed, for example, the Riemann solver AUSMDV presented from Wada and Liou in [18,19], which concerns substantially a combination of two methods and was used in this work.

A substantial characteristic of the Riemann solvers AUSMDV is the accurate reproduction of the flux over contact discontinuity, flux over shocks is not accurately reproduced, which is less important for numerical modeling.

With this Riemann solver, the numerical experiments show in [19] that a durable and vibration-free can possibly describe the shock waves and expansion waves.

By the convection most physical quantities are transported only passively with the mass. For this reason, by the AUSMDV one tries to particularly exactly describe the total mass flux over the edge of a control volume. One can get the other convective flux by multiplication of the total mass flux with the respective passively transported magnitudes of the control volume.

3.5. Discretization of the source term

Because the additional energy equation of the species i (8) does not have a conservative form, a problem arises since the volume integral over the two last terms cannot be directly approximated as flux by the Riemann solver AUSMDV, but the source term must be discretized. As approximation of the volume integral, the cell average value is evaluated

$$\bar{Q}(x) = -\left(\bar{Y}_i \bar{u} \frac{\partial}{\partial x} P + \frac{\bar{P}_i \bar{P}}{\bar{\gamma}_i \sum_{j=1}^{ns} \frac{\bar{P}_j}{\bar{\gamma}_j}} \frac{\partial}{\partial x} u \right), \tag{24}$$

where the pressure gradient $\partial P/\partial x$ and the velocity gradient $\partial u/\partial x$ must be still discretized.

The two gradients $\partial P/\partial x$ and $\partial u/\partial x$ are first discretized by a one-sided method

$$\frac{\partial P_i}{\partial x} = \frac{P_{i-1} - P_i}{x_{i-1} - x_i} \quad \text{and} \quad \frac{\partial u_i}{\partial x} = \frac{u_{i-1} - u_i}{x_{i-1} - x_i}. \tag{25}$$

To improve the discretization of the source term, afterwards, they should be discretized by a double-sided method

$$\frac{\partial P_i}{\partial x} = \frac{P_{i-1} - P_{i+1}}{x_{i-1} - x_{i+1}} \quad \text{and} \quad \frac{\partial u_i}{\partial x} = \frac{u_{i-1} - u_{i+1}}{x_{i-1} - x_{i+1}}. \tag{26}$$

4. Results of the numeric computations

In this work we present the results for different test problems:

- *Propagation of a contact discontinuity between two different gases:*
  First, the usual mixture formula for γ (12) is investigated; in addition, the solutions of first and second order are discussed. Afterwards the dependence of the disturbances are shown by the spatial and temporal resolution and by the temperature and gamma conditions over the initial discontinuity. At the end, the influence of the general mixture formula for γ (9) is studied, and compared with the above results. We will denote the two methods in the following sections in the following ways:
  - *old modeling:* the simple conservative equation for the partial density (2) with the usual mixture formula for γ (12)
  - *new modeling:* the additional energy equation of the species (8) with the general mixture formula for γ (9)
- *A shock tube with two different gases:*
  In this test case, the results of above both modelings will first be compared. Afterwards, the problems of the new modeling will be shown in this paper too, it includes the restrictions and difficulties on the additional energy equation of a species.

The effects of the boundary conditions on the solution are significant in principle, however they are not treated in this work, since the computations are broken off and become apparent before the changes of the solution at the edges.

4.1. Propagation of a contact discontinuity

We study the convection of a contact discontinuity, which two different gases – air (species 1, $\gamma = 1.4$ and mol mass $W = 28.97$) and helium (species 2, $\gamma = 1.667$ and mol mass $W = 4.0$) – are separated from each other. The accomplished numerical experiments for the simulation of a spatially one-dimensional propagation of the contact discontinuity are based on the initial conditions given in Table 1.

Table 1
Initial conditions of the contact discontinuity.

	ρ_1	ρ_2	u	p	Y_1	Y_2	x
Left (l)	1	0	1	1	1	0	$x < 0.25$
Right (r)	0	0.5	1	1	0	1	$x \geq 0.25$

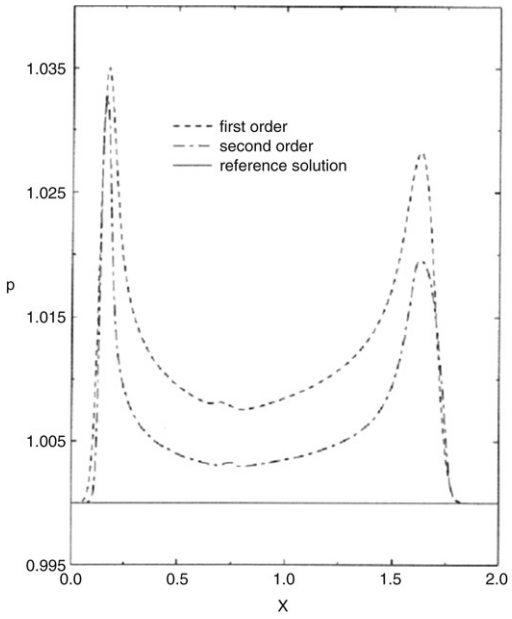

Fig. 3. Comparison of the orders with the old modeling in the pressure field.

Here x varies on the distance from 0 to 2. The pressure and the velocity remain constant; we use the spatial discretization $\Delta x = 0.01$; the distribution of the initial values for $U_l = U(x < 0.25)$ and $U_r = U(x > 0.25)$ and the time integration ends by $t = 0.5$.

4.1.1. Results of first and second order approximation

The Fig. 3 shows the comparison of the results of two different orders. The solutions are produced with the old modeling (see Section 2.3). The solutions at time $t = 0.5$ represent the contact discontinuity at the place $x = 0.75$. The broken and the point-broken lines mark the solutions of first and second order. The continuous line marks the reference solution.

In the Fig. 3 one recognizes that there is approximately 3 per cent error in the pressure field. The two moving maxima of the error lie in the places $x_1 = 0.19$ and $x_2 = 1.65$ respectively. Their situations are given through

$$x_1 = 0.25 + t\,(u_l - c_l) \quad \text{and} \quad x_2 = 0.25 + t\,(u_r + c_r). \tag{27}$$

Except for the two maxima, one can still recognize the small disturbance by the place of the contact discontinuity $x = 0.75$.

The results with second order accuracy to the space and time point show in the same figures that the discontinuity is better solved. The non-physical disturbances of the pressure turn out to be smaller by high order. For this reason, all the following solutions are produced with the second order procedure. Although the disturbances of all variables are better solved in this case, the maxima still remain clear.

4.1.2. Problems with the old modeling

1. *Propagation of the disturbances*

   The discussed disturbances of the variables were pointed only to the time $t = 0.5$ before. In order to recognize the propagation of the disturbances, in the Fig. 4, the pressure distributions are shown at different times.

   The two large disturbances spread clearly to the left and right, i.e., they do not remain constant in the same place. The right propagation is faster than the left, there the disturbances spread to the right with a propagation velocity $u_r + c_r \approx 2.8$ and to the left $u_l - c_l \approx -0.18$. Although the propagation of the left disturbance is not so fast, one can clearly recognize the tendency nevertheless.

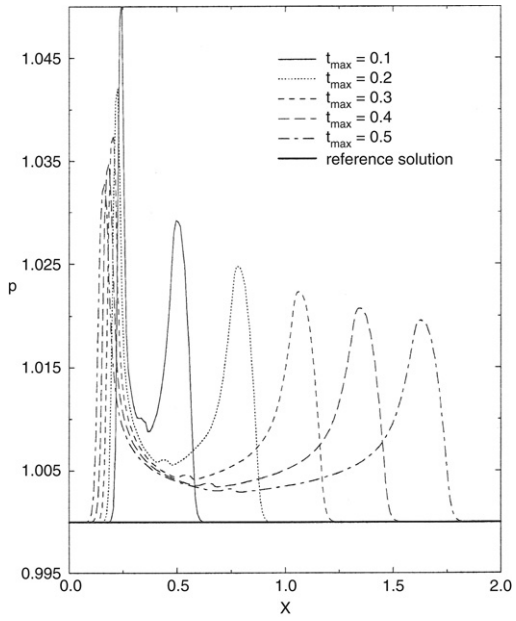

Fig. 4. Comparison of the disturbance propagation with time in the pressure field.

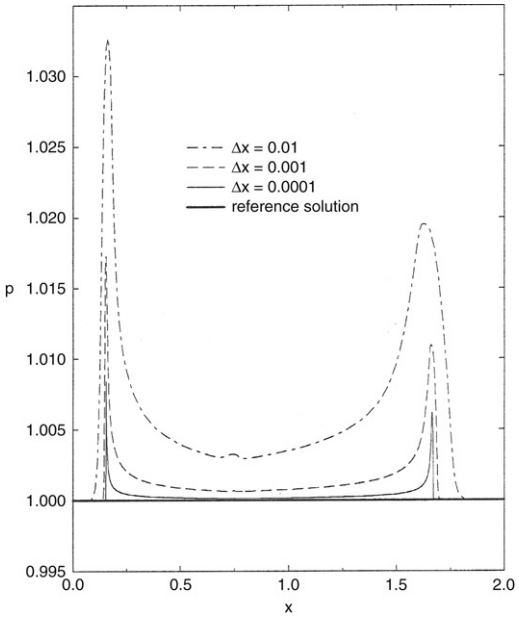

Fig. 5. Influence of the spatial dissolution on the pressure.

2. *Influence of the spatial discretization*
   In this part, the influenced variable of the number of cells is presented. The results of the computation are represented in the Fig. 5.
   In this test, three different spatial discretization Δx are investigated, their values are individually 0.01, 0.001 and 0.0001. The numerical disturbances in the pressure field point out that the numerical simulation in the flow field is improved by the refined grids. But the falling tendency of the maxima also shows that they do not reduce proportionally to the spatial discretization by 10-fold directly, but they decrease only by approx. 2-fold.
3. *Influence of temporal resolution*
   In this part, the influence of temporal resolution is tested. The results are represented in the Fig. 6. In this test, three different temporal resolutions are used. We use 0.8, 0.08 and 0.008 as CFL-numbers. In the figure, it shows that temporal resolution does not have a large influence on the numerical disturbances.

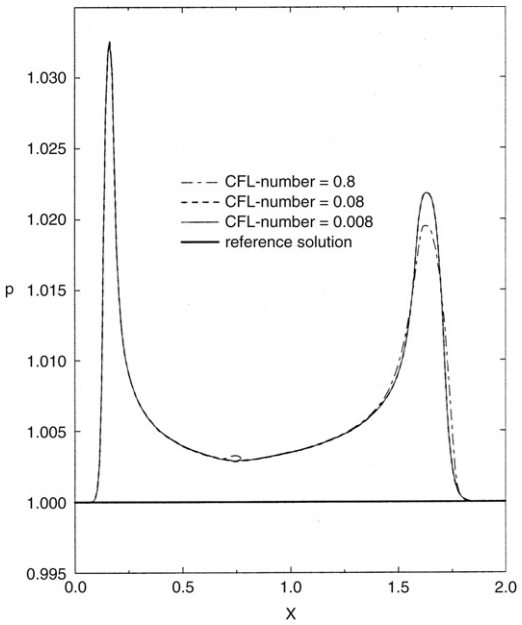

Fig. 6. Influence of the CFL-number on the pressure.

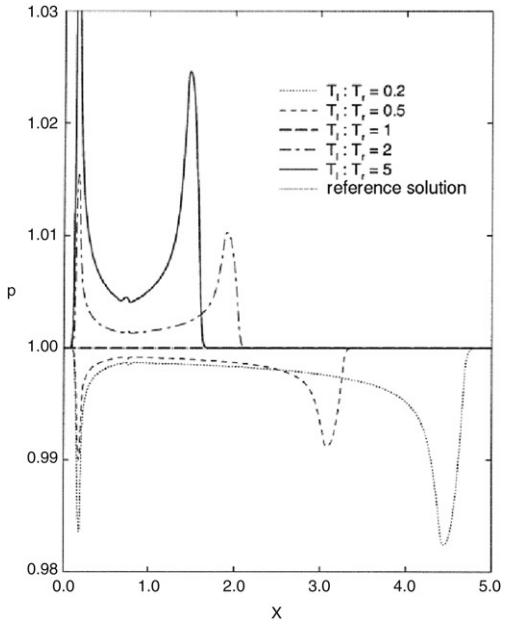

Fig. 7. Influence of the temperature jump on the pressure distribution.

4. *Influence of the temperature jump*

As the next influenced variable, the temperature jump is carried out in this part and represented in the Fig. 7. Five different temperature jumps are investigated in this test with values 0.2, 0.5, 1, 2 and 5. The densities are determined as follows

$$P_l = \frac{\rho_l R T_l}{W_l} = \frac{\rho_r R T_r}{W_r} = P_r,$$
$$\frac{T_l}{T_r} = \frac{\rho_r}{\rho_l}\frac{W_l}{W_r}. \tag{28}$$

Conditions are summarized in the Table 2.

The Fig. 7 shows: If the temperatures of both gases are equal in a cell, the results of the computation coincide with the reference solution. If the two temperatures are different in a cell, numerical disturbances arise. This result is consistent

Table 2
Data for temperature jump.

T_l/T_r	ρ_l/ρ_r	W_l/W_r	ρ_r
0.2	35	7	0.02857
0.5	14	7	0.07143
1.0	7.0	7	0.14286
2.0	3.5	7	0.28571
5.0	1.4	7	0.71429

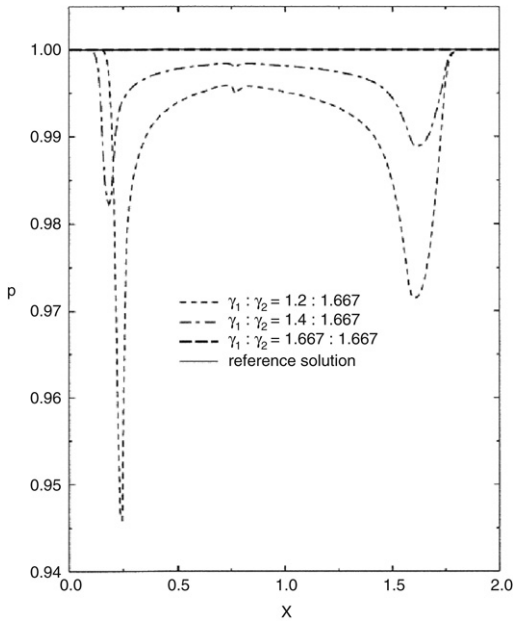

Fig. 8. Comparison of the pressure distribution for different γ-jumps.

with the condition for the old modeling in Section 2.3. The disturbances have a tendency to grow with the temperature jump. The temperature jump has a strong influence on the disturbances.

5. *Influence of γ-jump*
As a further influenced variable, the γ jump is tested in this part, and is represented in the Fig. 8. In this test, three different γ jumps are investigated. This experiment is accomplished on the assumption of same mol masses 28.97 for both gases. In the figure, it shows clearly that the results with the same γ-values coincide well with the reference solution. Moreover, the results have the tendency that the numerical disturbance increases with larger γ-jump.

4.1.3. New modeling

The new model is computed under the same conditions as the old model in this part. The results are represented in the Figs. 9 and 10.

The two figures show that the results of the new modeling agree outstandingly with the reference solution. The pressure and the density in the figures are identical to the reference solution. That is, their distributions are constant without non-physical disturbances. In addition, the movement of the contact discontinuity is better predicted in this case.

4.2. The shock tube with two different gases

In this part we study a shock tube as a test problem, in which three different wave propagations take place, which are in an individual expansion wave, a contact discontinuity and a shock wave. At the beginning, two different gases are separated in the shock tube by a membrane — air (species 1, $\gamma = 1.4$ and mol mass $W = 28.97$) at the left side and helium (species 2, $\gamma = 1.667$ and mol mass $W = 4.0$) at the right side. The initial conditions are given for this case in the Table 3.

Here x varies with the distance from 0 to 1. For the spatial discretization we use $\Delta x = 0.01$ according to homogeneous control volumes. The time integration ends by $t = 0.33$.

4.2.1. Comparison of old and new models

The comparison of the models is represented in the Figs. 11 and 12. An individual contact discontinuity and a shock wave are recognized by the places $x = 0.65$ and $x = 0.836$. The initial data are selected in such a way that a large jump of

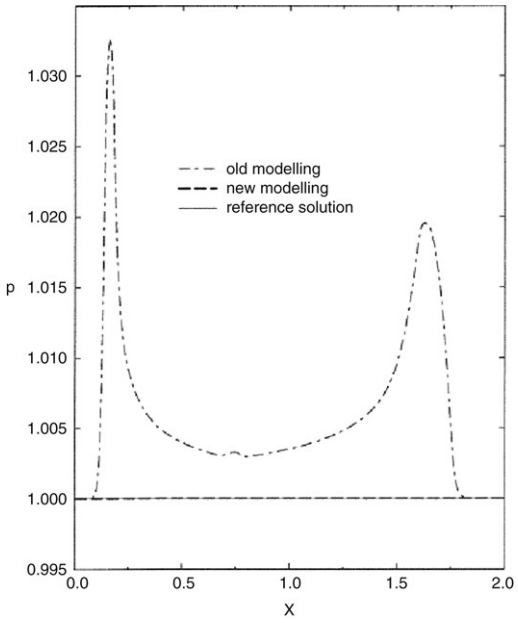

Fig. 9. Comparison of the models by pressure.

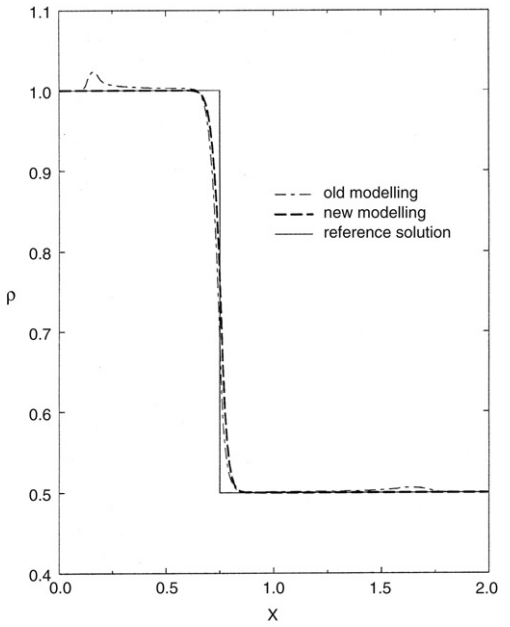

Fig. 10. Comparison of the models by density.

Table 3
Initial conditions of the shock tube problem.

	ρ_1	ρ_2	u	p	Y_1	Y_2	x
Left (l)	1	0	0	1	1	0	$x < 0.5$
Right (r)	0	0.8	0	0.2	0	1	$x \geq 0.5$

temperature is presented over the contact discontinuity. In this way one can surmise that a numerical error arises from the treatment of the discontinuity with the old model. This assumption is clearly confirmed in the pressure- and density-fields. The results of the new model do not show this numerical error, the results are in good correspondence with the reference solution.

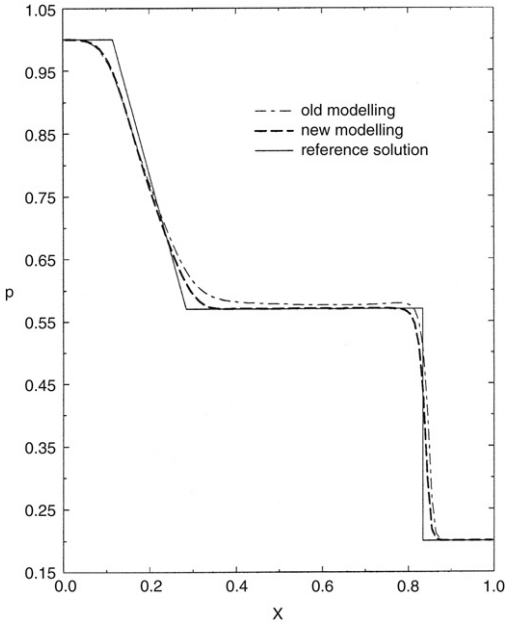

Fig. 11. Comparison of the models of the shock tube by pressure.

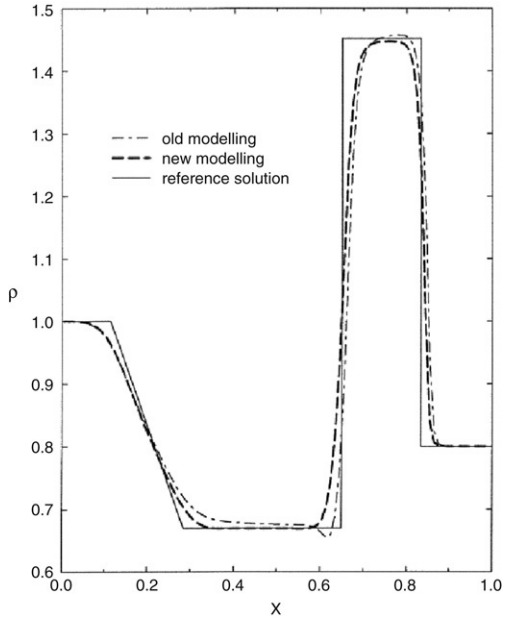

Fig. 12. Comparison of the models of the shock tube by density.

4.3. Problems of the discretization of the source term

The numerical results described before show that the numerical errors are improved by the suggested modifications. Although the non-physical disturbances in the variables, which describe the gas mixture, can be avoided by this modification, the additional equations show still some problems by the numerical approximation of the species variables. We discuss such problems in the following sections.

4.3.1. The approximate error before the contact discontinuity

We examine a problem from the last Section 4.2. An enlargement of the distribution of the gamma variables shows slight fluctuations for the new model in the Fig. 13. Because the general mixture formula for γ (9) depends on the partial pressure

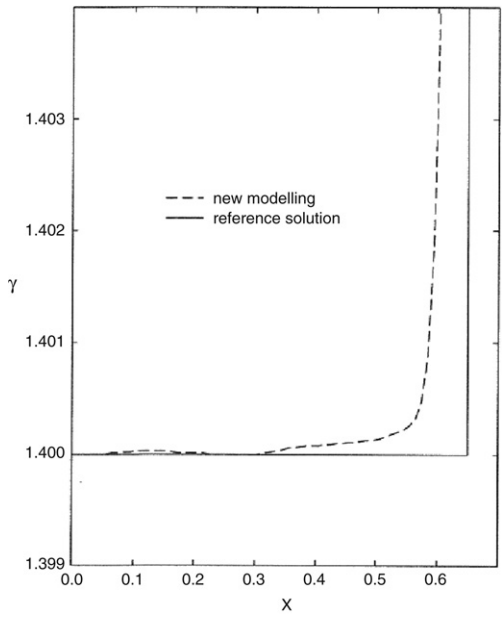

Fig. 13. The approximate error before the contact discontinuity in γ-field.

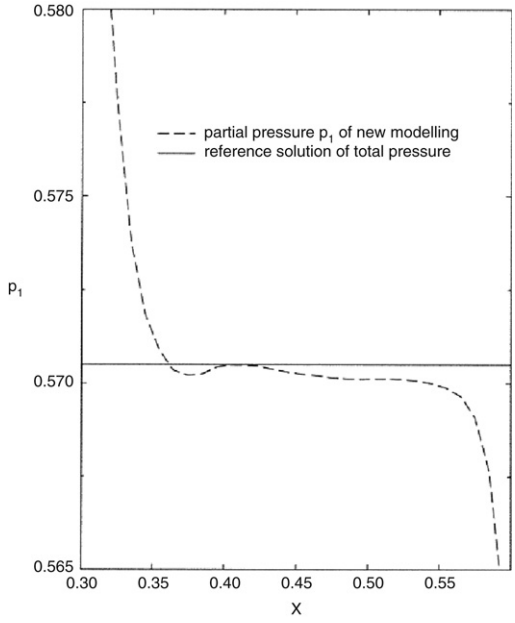

Fig. 14. The approximate error before the contact discontinuity in the partial pressure.

P_i of the species, whose results we must here also know therefore, the partial pressure P_1 is also represented in the Fig. 14. The figure shows that the partial pressure P_1 oscillates within the range between the expansion wave and the shock wave. In order to recognize this error correctly, we must also test another initial condition in the following section.

4.3.2. The problem of the gradients in the discretization of the source term

In order to find the weaknesses of the new model, we study the discretization of the source term. Since the gradients of the flow parameters are largest over the shock, the source term will arise in the nearby of discontinuity. In order to represent the difficulties, the initial conditions of the shock tube problem are appointed for one species and described in the Table 4.

Only one gas – air (species 1, $\gamma = 1.4$ and mol mass $W = 28.97$) – is thereby used, the second species – helium – is completely switched off in this case. Under these conditions, the numerical results of the additional energy equation of a species (8) should agree with the results of the conservative equation for the total energy (4).

Table 4
Initial conditions of the shock tube problem for only one species.

	ρ_1	ρ_2	u	p	Y_1	Y_2	x
Left (l)	1	0	0	1	1	0	$x < 0.5$
Right (r)	0.8	0	0.2	0	1	0	$x \geq 0.5$

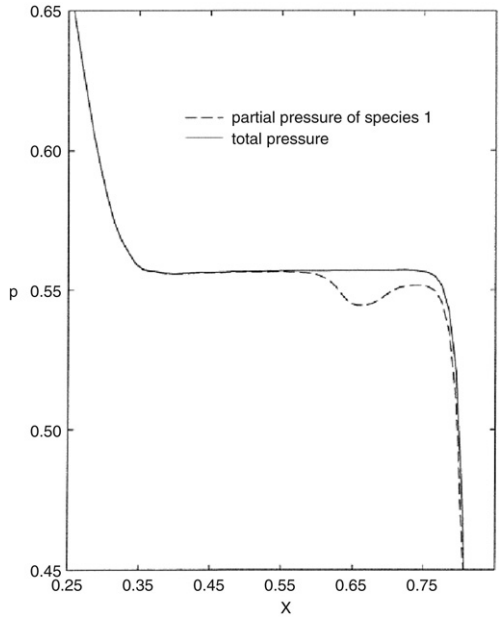

Fig. 15. Comparison of the total pressure and the partial pressure of a species.

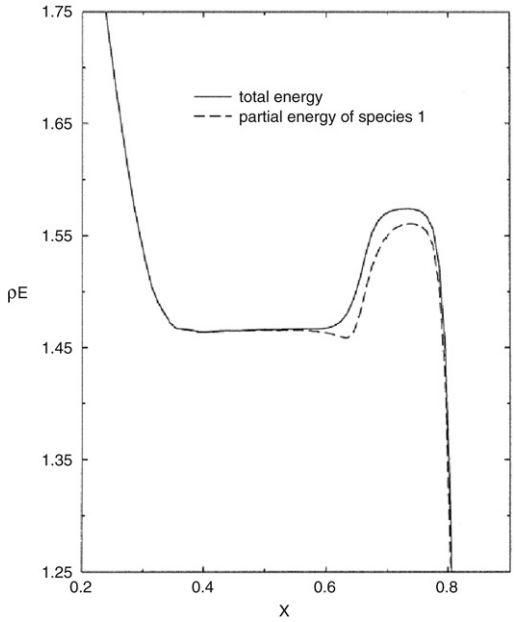

Fig. 16. Comparison of the total energy and the partial energy of a species.

To solve the general mixture formula for γ (9), we need the partial pressures P_i and for the total energies of the species $\rho_i E_i$. Both magnitudes are presented in the Figs. 15 and 16.

In the figures the comparisons of both magnitudes show that the partial pressure P_i and the total energy of a species $\rho_i E_i$ do not agree with the total pressure P and the total energy ρE.

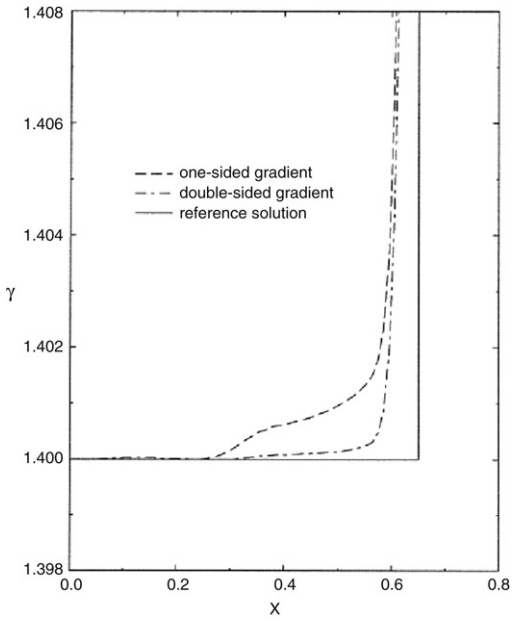

Fig. 17. Comparison of one-sided and double-sided methods.

We can summarize here briefly that the discretization of the source term in the Eq. (8) and that it has still some unclear problems with the non-conservative formulation.

The problem of different gradient discretizations

In the Section 3.5 two different methods for the discretizations of the gradients of P and u in the source term are described, denotes as one-sided method (25) and double-sided method (26). The difference between both methods in the distribution of the γ variables are represented in the Fig. 17.

The Fig. 17 represents a cutout in the distribution of this picture, in which the two methods differ from each other before the contact discontinuity. Here the gradients in the source term, the double-sided method approximates better than the one-sided method.

5. Conclusions

In the context of this work is detailed to treat the unsteady, one-dimensional Euler equations for gas mixtures with an additional conservative equation.

The numerical results of the model with a simple conservative equation for the partial density (2) and the usual mixture from (12) for γ show clearly as a result, with this model the numerical disturbances arise near the contact discontinuities and shocks at different temperatures of all gases. The produced disturbances spread to the left and right respectively with time. The non-physical disturbances depend strongly on the spatial discretization, the temperature jump and γ-jump of both gases as well as on the temporal discretization.

The numerical results of the model by the additional energy equation of the species (8) with the general mixture form (9) for γ shows from the results, that the conservative field variables agree outstandingly with the reference solutions. The disturbances can be eliminated with such a model. In this case, the form (9) is directly dependent on the partial pressure P_i, which we need in the additional energy equation of the species (8) to estimate the values of γ. But the numerical distribution of such a model shows still lighter disturbances, which have their cause in the non-conservative formulation of the additional energy equation of the species and the associated treatment of their source terms.

This model represents a very good and consistent formulation for the numerical simulation of contact discontinuity between different gases, it allows different temperatures by the gases involved within a cell. However, for example the treatment of moving contact discontinuity remains open, with which all gas components are already mixed on the both sides of the discontinuity. In such a case, a treatment for the real temperatures and the real partial pressures on such positions from the restudying additional energy equation of the species is desirable in future work.

Acknowledgments

We want to thank to Prof. G.E.A. Meier, Prof. Walter Riess of the Institute of Turbomachinery and Fluiddynamics of University Hannover and Prof. Tong Yang of the Department of Mathematics of City University of Hong Kong as well as in particular Dr. Volker Hannenmann of the Institute of Aerodynamics and Flow Technology of German Aerospace Center for

their continuously encouragement and their helpful discussions to this work for the writing, to the referee for their interest and very helpful comments to this work.

References

[1] R. Abgrall, How to prevent pressure oscillations in multicomponent flow calculations: A quasi conservative approach, Journal of Computational Physics 125 (1996) 150–160.
[2] Renjun Duan, Meng-Rong Li, Tong Yang, Propogation of singularities in the Boltzmann equation near equilibrium, Mathematical Models and Methods in Applied Science 18 (7) (2008) 1093–1114.
[3] P. Jenny, B. Mueller, H. Thomann, Correction of conservative Euler solvers for gas mixtures, Journal of Computational Physics 132 (1997) 91–107.
[4] K.M. Shyue, An efficient shock-capturing algorithm for compressible multicomponent problems, Journal of Computational Physics 142 (1998) 208–242.
[5] V.T. Ton, Improved shock-capturing methods for multicomponent and reacting flows, Journal of Computational Physics 128 (1996) 237–253.
[6] K. Xu, BGK - based scheme for multicomponent flow calculations, Journal of Computational Physics 134 (1997) 122–133.
[7] J.D. Anderson Jr., Modern Compressible Flow, McGraw-Hill, 1990.
[8] J.D. Anderson Jr., Computational Fluid Dynamics, McGraw-Hill, 1995.
[9] R.W. Fox, A.T. McDonald, Introduction to Fluid Mechanics, John Wiley and Sons, 1994.
[10] J.E.A. John, Gas Dynamics, Allyn and Bacon, 1984.
[11] B. Noll, Numerische Strömungsmechanik, Springer-Verlag, 1993.
[12] R.H.F. Pao, Fluid Dynamics, Charles E. Merrill Books, 1973.
[13] T.-H. Shieh, Technical report & Thesis, Section of Aerothermodynamics of Institute for Fluidmechanics of German Aerospace Center (DLR) & Institute for Turbomachinery and Fluiddynamics of University Hannover, 1999.
[14] W. Kordulla, Numerische Simulation in der Strömungsmechanik, in: Lecture Notes, Institute for Turbomachinery of University Hannover, 1999.
[15] V. Hannemann, Numerische Simulation von Stoß-Stoß- Wechselwirkungen unter Beruecksichtigung von chemischen und thermischen Nichtgleichgewichtseffekten, DLR-Forschungsbericht 97-07, 1997.
[16] C.B. Laney, Computational Gasdynamics, Cambridge University Press, 1998.
[17] W. Wegner, Vollständige Riemannlösung der ein- und zweidimensionalen Euler-Gleichungen, DLR-Forschungsbericht 92–93, 1992.
[18] M.-S. Liou, C.J. Steffen, A flux splitting scheme, NASA TM104404, 1991; J. Comput. Phys. 107 (1993) 23–39.
[19] Y. Wada, M.-S. Liou, A flux splitting scheme with high-resolution and robustness for discontinuities, AIAA-94-0083, 1994.